TWIN-SHAPED CFRP-SANDWICH PEDESTRIAN BRIDGE

F. Broggini [1], L. Diviani [2], D. Rüegg [3], M. Ambrosini [4] and T. Keller [5]
[1] Blueoffice Architecture, Bellinzona, Switzerland
[2] University of Applied Sciences and Arts of Southern Switzerland (SUPSI), Manno, Switzerland
[3] Ernst Basler + Partner AG, Zurich, Switzerland
[4] BASE Srl., Alserio CO, Italy
[5] Ecole Polytechnique Fédérale de Lausanne (EPFL), Lausanne, Switzerland

ABSTRACT

A concept of a nature-inspired pedestrian bridge which tries to merge architectural, structural and manufacturing aspects in an optimized way is presented. The 18.0-m-span bridge is designed as an overhead spatial frame of a complex double-curved shape, which is composed of twelve modules consisting of lightweight carbon fiber-reinforced polymer (CFRP) sandwich construction. The modules are fabricated with only one mould through vacuum assisted resin infusion. The aimed visible texture and black colour of the CFRP fabrics represents an essential architectonical element. The resulting benefits and required compromises of this multi-criteria approach are discussed.

KEYWORDS

CFRP, bridge, module, sandwich.

INTRODUCTION

The new 18.0-m-span TSCB (twin-shaped composite beam) pedestrian bridge connects the villages of Bissone and Melide on the eastern and western side of the lake of Lugano in Switzerland. The architectural and structural concept is inspired by natural microorganisms, e.g. radiolarians and diatoms, whose skeletons are structurally optimized lightweight constructions. The resulting bridge structure is conceived as an overhead spatial frame of 2.40-m height, as shown in Figures 1 and 2. The roof frame and walkway slab are in parallel, horizontal planes while the side frames are undulated and form three waves of 6-m length each, see Figures 3 and 4. This undulation results in an also undulating width of the roof frame and walkway slab along the bridge, which are staggered however by one half-wave length, i.e. in the cross sections with the largest width of the walkway slab the width of the roof frame is the smallest and vice versa. The width of the walkway thus varies between 1.36 and 3.36 m. The edges between the horizontal and the undulated side frames are double-curved. Furthermore, transverse stiffeners are located around the frame openings to increase the buckling resistance of the compressed frame struts.

Figure 1 Rendering of TSCB bridge

Following the aim of approaching the efficiency of natural structures, the components of the lightweight spatial frame are conceived in sandwich construction. Carbon fiber-reinforced polymer (CFRP-) materials were selected for the face sheets since the architectural concept aimed to have a black coloured bridge with a surface finish that shows the texture of the fabrics.

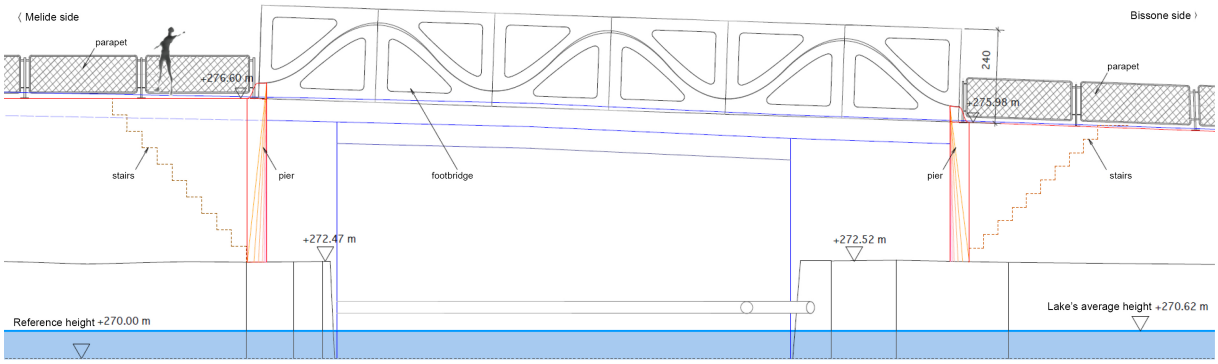

Figure 2 Bridge elevation (dimensions in [cm])

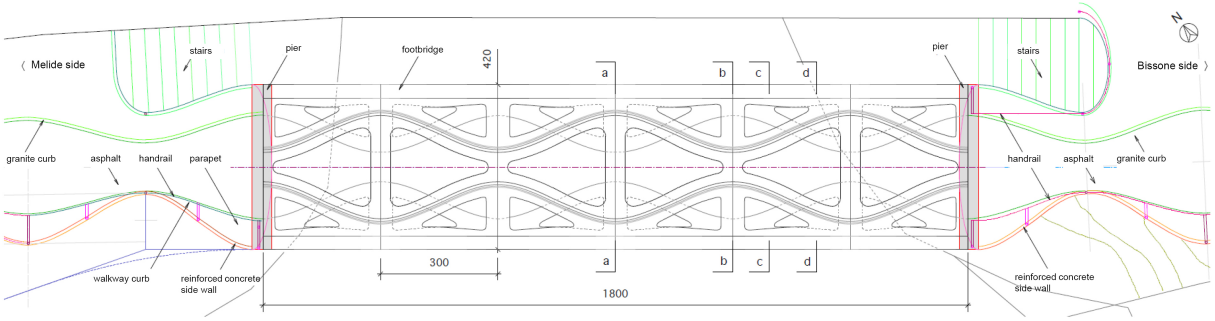

Figure 3 Plan view (dimensions in [cm])

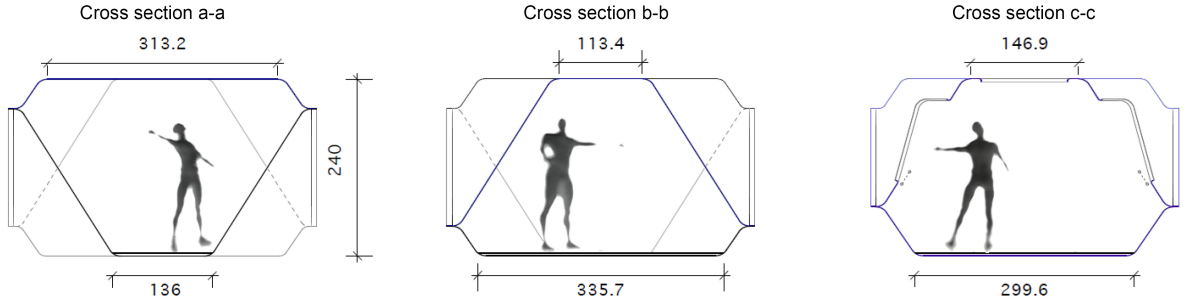

Figure 4 Cross sections (dimensions in [cm]; cross sections are indicated in Figure 3)

The geometry of the bridge was not only a result of the architectural and structural conception, but also optimized from the manufacturing point of view. The overall complex shape is conceived in a way that it can be built up from only one complex module of 3.0-m length, as shown in Figure 5, which requires only one (expensive) mould for manufacturing. The openings in the bottom frame are closed to form the walkway slab. Furthermore, the undulating joints between the upper and lower modules are located in vertical planes to reduce the geometrical complexity, see Figure 4; the overall bridge width is thus constant (4.20 m), see Figure 3. Vacuum assisted resin infusion was selected for the manufacturing with the mould being placed on the inner side to have the smooth surface there. All the joints are vacuum infused or adhesively-bonded in the factory; the whole bridge is thus prefabricated and transported to the site.

MATERIALS AND STRUCTURAL MODEL

The thickness of the roof and side frame sandwiches is 30 mm, and that of the walkway slab 40 mm. The CFRP face sheets are 0.75-mm thick and composed of three layers of fabrics (SAATI CC283, 49/51% in 0/90° direction) and an epoxy resin (Conchem LC 318/IN). Lightweight (280-g/m^2) twill-weave fabrics were selected due to the required drapability. The three layers are rotated against each other by 30° (arranged at 0/30/60°) to form quasi-isotropic laminates since an anisotropic lay-up, that would better adapt to the stress fields, was inconceivable considering the complex geometry. The 3-layer laminates are thus asymmetric, the resulting

through-thickness stresses in the core are however insignificant. The laminate lay-up is doubled to 6 layers (in a symmetric arrangement) in the walkway slab and, in the curved edge regions marked in yellow in Figure 6, it is increased to 6 or 12 layers. The laminates are UV-protected by a transparent coating. The core material is an orthotropic polyethylene terephthalate (PET) foam of 135-kg/m^3 density (Airex T92.130). The foam is placed with the extrusion direction and weldline planes perpendicular to the face sheets (in ″end-grain″ direction). The foam is substituted by an isotropic solid polyurethane (PUR) material (SikaBlock M930) in the support cross beams (blue region in Figure 6) and the double-curved curved edge regions.

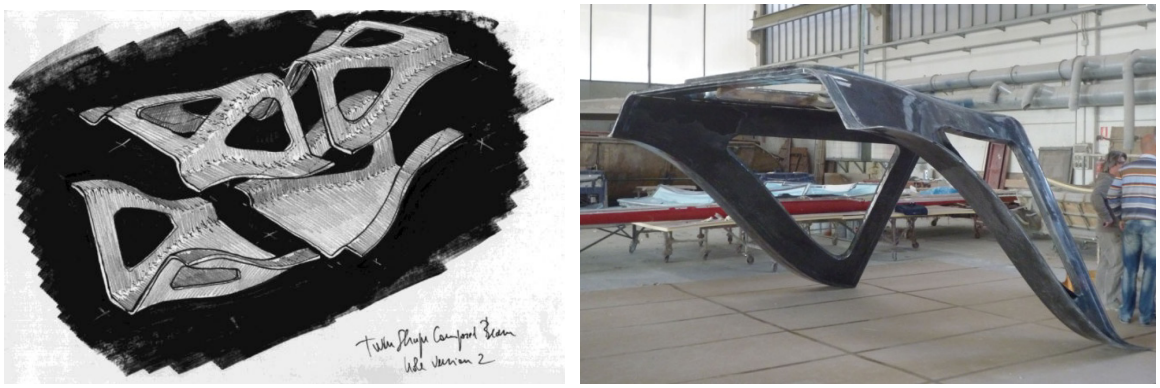

Figure 5 Twin-shape concept and prototype of basic module

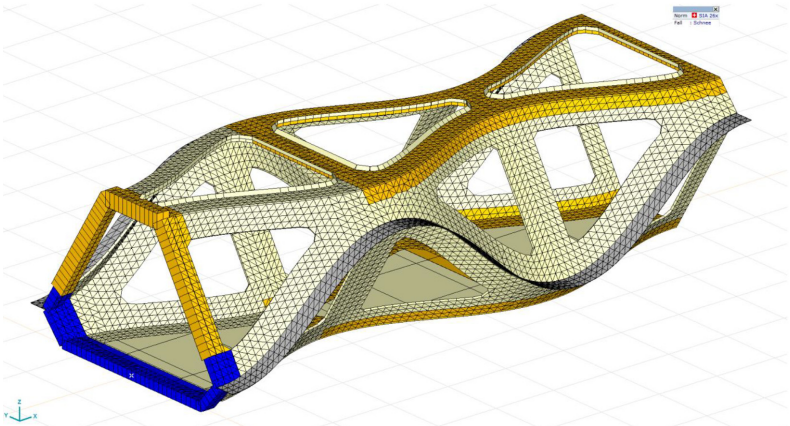

Figure 6 Structural model (half of the total length, support on the left side)

The laminate properties and joint strengths were obtained from testing, the core properties from the manufacturer. The main properties of the CFRP laminates and PET foam at room temperature are given in Tables 1 and 2. Due to the black colour, the surface temperature could locally increase up to 84°C, as corresponding measurements on CFRP sandwich samples protected with a transparent UV-coating and exposed to a normal irradiation of 1000 W/m^2 (as present in Bissone) have shown. The maximum allowable service temperature, however, was defined as the onset value of the glass transition temperatures, $T_{g\text{-}onset}$ (according to dynamic mechanical analysis, DMA), of the resin or foam minus 10°C. Surfaces which would exceed this temperature are painted with a light colour to limit the temperature increase to the allowable temperature.

The replacement of the PET foam in the strongly curved edge regions by the solid PUR material was necessary since the foam could not be placed in end-grain direction. A deviation of this direction, however, was linked with a drop of the properties due to the material orthotropy. Several core materials were evaluated to solve this problem, as it is shown by a comparison of some significant properties listed in Table 3. A comparable high-density (almost) isotropic polyurethane foam (PUR 145) has a better tensile strength than the selected PET foam transverse to its extrusion direction (index $\perp$), however, the properties parallel to the PET foam extrusion direction (index $\parallel$) were much lower. Orthotropic Balsa wood, on the other hand, has much better properties in grain direction than the PET foam in extrusion direction. However, the tensile strength in the critical transverse direction is lower. It was thus not possible to find only one lightweight material (at a reasonable cost) that would fulfil all the requirements and the selected two-material solution resulted as being the best one.

Table 1 CFRP laminate properties

Property	3-layer asymmetric	6-layer symmetric	Notes
Orientation	0/30/60°	0/30/60/60/30/0°	
Thickness, t_L (mm)	0.75	1.50	
Tensile strength, $f_{Lt,k}$ (MPa) [1]	290	520	in 15°-direction
Elastic tensile modulus, $E_{Lt,k}$ (MPa) [1]	24200	45300	Average value
$E_{Lt,m}$ (MPa) [2]	31700	51200	0/15°-directions
Tensile failure strain, $\varepsilon_{Lt,k}$ (%) [2]	1.6	1.5	Average value 0/15°-directions
Poisson ration, ν_L (-)	0.32	0.32	Calculated value
Thermal elongation coefficient, α_m (K^{-1}) [2]	13.6E-6	17.5E-6	in 0°-direction

[1]characteristic, [2]average values

Table 2 PET foam properties

Property	Values	Notes
Tensile strength, $f_{Ct,k}$ (MPa) [1]	2.11	Extrusion direction
Compression strength, $f_{Cc,k}$ (MPa) [1]	2.15	Extrusion direction
Shear strength, $\tau_{C,k}$ (MPa) [1]	1.14	Extrusion direction
Elastic modulus, $E_{C,m}$ (MPa) [2]	50	⊥ to extrusion direction, FEM
Elastic modulus, tension, $E_{Ct,k}$ (MPa) [1]	138	Extrusion direction, wrinkling verification
compr., $E_{Cc,k}$ (MPa) [1]	115	
Shear modulus, $G_{C,k}$ (MPa) [1]	26	Extrusion direction, wrinkling verification
Poisson ration, ν_C (-)	0.30	Assumed value
Thermal elongation coefficient, $\alpha_{C,m}$ (K^{-1}) [2]	76E-6	⊥ to extrusion direction

[1]characteristic, [2]average values

Table 3 Core material comparison

Property	PUR 145 (Keller et al. 2008)	T92.130 end-grain	Balsa end-grain (Keller et al. 2014)
Density, ρ (kg/m³)	145	135	250
Tensile strength, $f_{Ct,\parallel,k}$ (MPa)	1.40	2.11	7.9
$f_{Ct,\perp,k}$ (MPa)	1.40	0.91	0.7
Shear strength, $\tau_{C,\parallel,k}$ (MPa)	0.70	1.14	2.3
Elastic tensile modulus, $E_{Ct\perp,m}$ (MPa)	55	175	200
Shear modulus, $G_{C,\parallel,m}$ (MPa)	21	30	290
Thermal elongation coefficient, $\alpha_{C,\perp,m}$ (K^{-1})	50E-6	76E-6	20E-6

∥-⊥ = parallel-transverse to extrusion/grain direction

The spatial frame is supported by two elastomer bearings on each side, the support conditions are those of a simple beam. In addition, all supports are secured against uplift since wind uplift forces may be higher than the dead load. The spatial frame was modelled in a finite element software using shell elements; half of the bridge was considered using a symmetry condition, as shown in Figure 6. The geometry was simplified, i.e. the curved edges in the cross section were modelled as sharp corners; detailed verifications demonstrated that this simplification is on the safe side.

STRUCTURAL VERIFICATIONS

The structural verifications are based on Swiss standards (SIA), which are in line with Eurocode standards. The ultimate limit (ULS) and serviceability limit (SLS) states were verified using the partial safety factor concept, i.e. applying load factors on the action and resistance factors on the material side. The actions, their combinations and associated load factors were determined according to SIA260 (2013) and SIA261 (2014). Actions taken into account were dead and live loads, snow, wind and temperature. Since resistance factors for FRP materials are defined neither in the Swiss standards nor in the Eurocodes, resistance factors from Eurocomp (Clarke 1996) were adopted, as it is in accordance with the Eurocode design philosophy.

Resistance Factors

The resistance factor, γ_M, according to Eurocomp is composed of three sub-factors, $\gamma_M = \gamma_{M1} \cdot \gamma_{M2} \cdot \gamma_{M3}$, which take the property source, manufacturing method, load duration and operating temperature into account. The sub-factors at ULS were selected as follows: $\gamma_{M1} = 1.15$ (properties derived from tests), $\gamma_{M2} = 1.20$ (vacuum infusion process, fully post-cured), $\gamma_{M3} = 1.20$ or 3.00 for short-term or permanent actions, resulting in $\gamma_M = 1.70$ or 4.10 for short-term or permanent actions. These factors were applied to the characteristic, i.e. 5%- fractile strength and stiffness values of the laminate and core materials in order to obtain the design values. The core and laminate stiffness values were used to calculate the wrinkling resistance of the laminates. For the verification of adhesively-bonded joints, a fourth factor, γ_{M4}, is applied. The four factors in this case are $\gamma_{M1} = 1.25$ (properties derived from tests), $\gamma_{M2} = 1.50$ (manual application, no adhesive thickness control), $\gamma_{M3} = 1.00$ or 1.50 for short-term or permanent actions, $\gamma_{M4} = 2.00$ (service conditions outside the adhesive test conditions), resulting in $\gamma_M =$ 3.75 or 5.60 for short-term or permanent actions.

At SLS, the average stiffness values were reduced by $\gamma_M = 1.30$ and creep was considered by a further stiffness reduction factor of 0.41 (Eurocomp, Figure 4.13, CSM/WR worst case at a 50-years' time). Furthermore, a strain limit of 0.2% was taken into account at SLS.

Ultimate Limit State

The laminate tensile and compressive resistances were verified, the latter according to the following wrinkling equation (Wiedemann 1996):

$$f_{w,d} = C_w \cdot \sqrt[3]{E_{L,\|,d} \cdot E_{C,\perp,d} \cdot G_{C,\perp,d}} \qquad (1)$$

with $f_{w,d}$ = design value of the wrinkling resistance, $C_w = 0.5$ (Keller et al. 2008), $E_{L,\|,d}$ = design value of the laminate elastic modulus, $E_{C,\perp,d}$ = design value of the core elastic modulus, $G_{C,\perp,d}$ = design value of the core shear modulus. Further verifications concerned the core shear stresses and the through-thickness stresses resulting in the curved regions, including laminate-core delamination.

For the stability verification of the compressed frame struts an initial deformation of 1/300 of the buckling length was assumed and a subsequent second order verification was performed.

Serviceability Limit State

SLS verifications concerned the deflections, vibrations (eigenfrequencies) and the above mentioned 0.2%-strain limit. The deflections were verified for permanent loads including creep and the live loads. The corresponding deflections limits according to SIA260 (2013) were span/700 and span/600 respectively, in both the longitudinal and transverse directions. Based on the sandwich composition resulting from the ULS verification, all the deflection limits were met with the exception of the deflection of the walkway slab at the largest width. The resulting deflection of span/300 however was assessed as being admissible.

Concerning vibrations, the eigenfrequencies of pedestrian bridges have to exceed 4.5 Hz for vertical and 1.3 Hz for horizontal (transverse) vibrations according to SIA260 (2013). The eigenmodes and eigenfrequencies were calculated taking the dead load and 10% of the live load into account. The resulting first and second eigenmodes are a lateral and a vertical vibration respectively, see Figures 7 and 8, at eigenfrequencies that exceed the limit values.

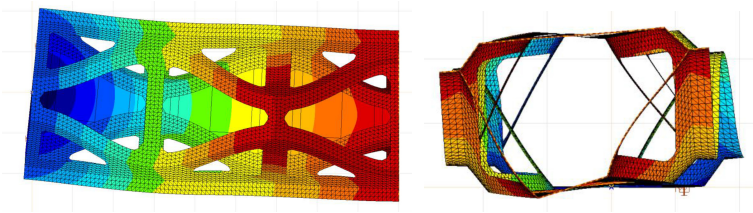

Figure 7 First eigenmode, lateral oscillation, 3.42 Hz eigenfrequency

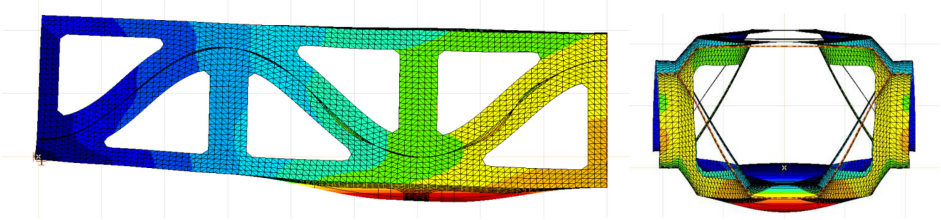

Figure 8 Second eigenmode, vertical oscillation, 4.64 Hz eigenfrequency

CONCLUSIONS

The intention of the new TSCB bridge is to create a bridge that meets architectural, structural and manufacturing requirements in an optimized way. The complex shape of the spatial frame can be built up of only one single module which can be manufactured in series. The overhead spatial frame has a large static height that offers a high stiffness and thus allows the laminate and core strengths to be fully used, which in most cases of FRP bridges is not possible due to deflection constraints. The complex, i.e. double-curved shape however also presents some disadvantages. The strength of the expensive carbon fibers cannot be fully used due to the required isotropic lay-up and orthotropic core materials are not ideal since their transverse direction is also stressed. Moreover, the small walkway width at mid-span results in high stresses in this cross section.

Without the architectural intention of exhibiting a black fabric texture and a slight increase of the frame static height and walkway core thickness, the bridge may be conceived at lower cost by using glass fibers. In fact, due to the temperature constraints, significant areas, in particular on the exterior side, need to be painted in a light colour. The selected sandwich construction, however, is an advantageous way to provide the required stiffness to prevent buckling in compressed parts and limit deflections in the walkway slab. Lightweight construction is thus maintained and the use of expensive CFRP materials is minimized. Furthermore, from the architectural point of view, the project demonstrates the liberty in the formal expression and plasticity offered by FRP composite materials.

ACKNOWLEDGEMENTS

The authors would like to acknowledge the funding of this project by the Swiss Federal Commission for Technology and Innovation CTI (Grant No. 7844.2) and the Canton of Ticino.

REFERENCES

Clarke, J. L. (1996). *Structural design of polymer composites – Eurocomp design code and handbook*, E & FN Spon, London, UK.

Keller, T., Haas, C. and Vallée, T. (2008). "Structural concept, design and experimental verification of a GFRP sandwich roof structure", *Journal of Composites for Construction*, 12(4), 454-468.

Keller, T., Rothe, J., de Castro, J. and Osei-Antwi, M. (2014). "GFRP-balsa sandwich bridge deck – concept, design and experimental validation", *Journal of Composites for Construction*, 18(2).

Swiss Society of Engineers and Architects (2013). *SIA 260: Basis of structural design*, SIA, Zurich, Switzerland.

Swiss Society of Engineers and Architects (2014). *SIA 261: Actions on structures*, SIA, Zurich, Switzerland.

Wiedemann, J. (1996). *Leichtbau 1: Elemente*, Springer, Heidelberg, Germany.